Supporting Information

Modulating structures to decouple thermoelectric transports leads to high performance in polycrystalline SnSe

Yuping Wang[1], Shulin Bai[1], Haonan Shi[1], Qian Cao[2], Bingchao Qin[1,*], Li-Dong Zhao[1,*]

[1] *School of Materials Science and Engineering, Beihang University, Beijing 100191, China.*

[2] *Huabei Cooling Device Co. LTD., Hebei 065400, China.*

Corresponding author: qinbingchao@buaa.edu.cn; zhaolidong@buaa.edu.cn

Experiment details

Samples preparation: All the samples in this work are on the basis of 2% Na doping. The high-purity elements Sn, Se, Ag, In, and Ge were weighed according to the stoichiometric ratio $(SnSe)_{1-x}(AgInSe_2)_x$ (x = 0.01, 0.015, 0.02, and 0.025), and $(Sn_{1-y}Ge_ySe)_{0.985}(AgInSe_2)_{0.015}$ (y = 0, 0.005, 0.0075, 0.01, and 0.0125) and for reactive materials such as Na, they are weighed in a glove box protected by an N_2 atmosphere. The resulting mixture of target weights is loaded into quartz tubes pre-coated with a carbon layer, evacuated to below 10^{-4} Torr and flame sealed. All samples were synthesized by the melt method. The sealed quartz tubes were then placed in larger diameter outer quartz tubes and subjected to the same evacuation and flame sealing operation to prevent oxidation of the product due to rupture of the inner tubes as a result of the phase change during the cooling process. The tubes were loaded into a muffle furnace and slowly heated to 1223 K for 12 h, then kept for 12 h, cooled to 793 K for 6 h, kept for 12 h, and then slowly cooled to room temperature in the muffle furnace. The obtained ingots were ground into powder with agate mortar, passed through a 200-mesh sieve, and then subjected to spark plasma sintering (SPS-211Lx) on a graphite mold with a diameter of 15 mm under an axial compressive stress of 50 MPa for 5 min at a vacuum of 773 K. Dense cylindrical samples with a size of $\Phi15$ mm × 8 mm were finally obtained, and then they were cut and polished to further measurements.

X-ray diffraction and Microstructure characterization: For the obtained samples, the physical phase structure should be analyzed and characterized firstly, and the macroscopic thermoelectric properties measured on the basis of physical phase analysis

have research value. The ingots were manually ground to a powder and then passed through a 200 mesh sieve used for phase analysis. The phase purity and identity were analyzed by the D/max 2500PC diffractometer equipped with Cu Kα (λ = 1.5418 Å) radiation.

Electrical transport properties: The samples were cut perpendicular to the pressure direction into rectangular samples of ~ 3 × 3 × 8 mm³ for simultaneous measurement of electrical conductivity and Seebeck coefficient of the samples over the temperature range of room temperature to 773 K under helium atmosphere using an Advance Riko ZEM-3 instrument to calculate the power factor data. The four-probe method is used, and the contact point between the sample and the probe is lined with carbon paper, which can effectively eliminate the influence of the contact resistance between the probe and the sample on the test results. The sample is coated with a thin layer of Boron Nitride (BN) to protect the instrument from possible damage caused by evaporation of the sample at high temperatures. The uncertainty of the Seebeck coefficient and conductivity measurements is within 5%. In addition to direct measurement of electrical conductivity and Seebeck coefficients, testing the carriers of a sample is an integral part of electrical property analysis. The carrier concentration and mobility of a sample can be tested by the Hall effect. The Hall coefficient (R_H) is measured by the Van der Pauw method using a Lake Shore 8400 device under a reversible magnetic field (test field strength 1T).

Thermal transport properties: The obtained samples were cut and polished into 6 mm diameter discs with uniform thickness in the range of 1 mm to 2 mm for thermal

diffusion coefficient (D) measurements. The D values in the room temperature to high temperature range were measured by laser flash method using a Netzsch LFA457 instrument made in Germany, and the thermal diffusion coefficient data were analyzed using a Cowan model with pulse correction. During the test, the top and bottom surfaces of the circular samples are coated with a thin layer of graphite to maximize the absorption of the laser signal by the sample and minimize errors due to material emissivity. The thermal conductivity of the material was calculated according to the equation $\kappa = D \times \rho \times C_p$, where ρ is the density of the sample determined using the sample dimensions and mass and verified using the Archimedes test method, and C_p is the specific heat of the sample, which is generally taken to be calculated according to Dulong-Petitlaw in this work. Taking into account all uncertainties in D, ρ and C_p, the uncertainty in the calculated thermal conductivity is within 8%. Combining all the uncertainties in the testing process of the thermal and electrical transport parameters, the uncertainty in the calculated ZT value is within 20%.

Callaway mopdel calculation method: The Callaway model can be used to identify the lattice thermal conductivity of material after introducing lattice imperfections into the matrix lattice, which is written as[1-2]:

$$\frac{\kappa_{\text{lat}}}{\kappa_{\text{lat}, p}} = \frac{\tan^{-1}(u)}{u} \qquad \text{\\* MERGEFORMAT (1)}$$

in which κ_{lat} and $\kappa_{\text{lat}, p}$ are the lattice thermal conductivities of the defected and parent materials, respectively. In this work, we use SnSe-AgInSe$_2$ as the parent material for calculation, in which $\kappa_{\text{lat}, p \text{ (SnSe-AgInSe2)}} = 1.23$ Wm^{-1} K^{-1}, u is defined as[3-4]:

$$u = \left(\frac{\pi^2 \theta_D \Omega}{h v_a^2} \kappa_{\text{lat}, p} \Gamma \right)^{1/2} \qquad \text{* MERGEFORMAT (2)}$$

$$\theta_D = \frac{h}{k_B} \left(\frac{3}{4\pi\Omega} \right)^{1/3} v_a \qquad \text{* MERGEFORMAT (3)}$$

$$v_a = \left[\frac{1}{3} \left(\frac{1}{v_l^3} + \frac{2}{v_s^3} \right) \right]^{-1/3} \qquad \text{* MERGEFORMAT (4)}$$

where θ_D, Ω, h, k, Γ, v_a, v_l, and v_s are the Debye temperature, average atom volume, Planck constant, Boltzmann constant, imperfection scattering parameter, average sound velocity, longitudinal sound velocities, and shear sound velocities respectively. The Γ is a weighted sum of the mass fluctuation (Γ_M) and strain field fluctuation (Γ_S), which can be written as:

$$\Gamma = \Gamma_M + \varepsilon \Gamma_S \qquad \text{* MERGEFORMAT (5)}$$

where is a phenomenological adjustable parameter related to the Poisson ratio (v_p) and Grüneisen parameter (γ)[5-6]. Moreover, ε, v_p, and γ can be expressed by[7]:

$$\varepsilon = \frac{2}{9} \left[(G + 6.4\gamma) \frac{1 + v_p}{1 - v_p} \right]^2 \qquad \text{* MERGEFORMAT (6)}$$

$$v_p = \frac{1 - 2\left(\frac{v_s}{v_l} \right)^2}{2 - 2\left(\frac{v_s}{v_l} \right)^2} \qquad \text{* MERGEFORMAT (7)}$$

$$\gamma = \frac{3}{2} \left(\frac{1 + v_p}{2 - 3v_p} \right) \qquad \text{* MERGEFORMAT (8)}$$

where G is a ratio between the relative change of bulk modulus and banding length. There is no change on the sites of Se after Ge substituting Sn sites, namely $\Gamma_{Se} = 0$. Thus Γ is defined as[8]:

$$\Gamma_{Sn_{1-y}Ge_ySe} = \frac{1}{2}\left(\frac{M_{(Sn,Ge)}}{\overline{M}}\right)^2 \Gamma_{(Sn,Ge)} \qquad \backslash* \text{ MERGEFORMAT (9)}$$

$$\overline{M} = \frac{1}{2}\left(M_{Sn} + M_{Ge}\right) \qquad \backslash* \text{ MERGEFORMAT (10)}$$

$$\Gamma_{(Sn,Ge)} = \Gamma_{M(Sn,Ge)} + \varepsilon\Gamma_{S(Sn,Ge)} \qquad \backslash* \text{ MERGEFORMAT (11)}$$

$$\Gamma_{M(Sn,Ge)} = y\left(1-y\right)\left(\frac{\vee M}{M_{(Sn,Ge)}}\right)^2 \qquad \backslash* \text{ MERGEFORMAT (12)}$$

$$\Gamma_{S(Sn,Ge)} = y\left(1-y\right)\left(\frac{\vee r}{r_{(Sn,Ge)}}\right)^2 \qquad \backslash* \text{ MERGEFORMAT (13)}$$

where $M_{(Sn,Ge)} = (1-y)M_{Sn} + Ym_{Ge}$, $\Delta M = M_{Sn} - M_{Ge}$ and $r_{(Sn,\,Ge)} = (1-y)r_{Sn} + yr_{Ge}$, $\Delta r = r_{Sn} - r_{Ge}$. Then we can obtain:

$$\Gamma_{Sn_{1-y}Ge_ySe} = \frac{1}{2}y\left(1-y\right)\left(\frac{M_{(Sn,Ge)}}{\overline{M}}\right)^2\left[\left(\frac{\Delta M}{M_{(Sn,Ge)}}\right)^2 + \varepsilon\left(\frac{\Delta r}{r_{(Sn,Ge)}}\right)^2\right] \backslash*$$

MERGEFORMAT (14)

Calculation method: All the first-principles calculations were performed with generalized gradient approximation (GGA) in combination with the projector augmented wave (PAW) method as implemented in the Vienna Ab initio Simulation Package (VASP)[9-10]. The Perdew–Burke–Ernzerhof (PBE) functional was used to describe the exchange-correlation energy[11]. A plane wave basis with a convergence kinetic energy cut-off of 400 eV was adopted in all calculations. The Brillouin Zone (BZ) was sampled using the Monkhorst-Pack k-mesh of $9 \times 6 \times 6$ with the energy convergence criterion of 10^{-6} eV. The crystals were fully optimized within the Hellmann-Feynman force convergence criterion of 10^{-2} eV/Å. A $1 \times 4 \times 4$ supercell ($Sn_{64}Se_{64}$) was constructed with two Sn atoms substituted by the In atom and Ag atom to model 1.5% In and 1.5% Ag alloying ($Sn_{62}AgInSe_{64}$). Considering the symmetry change due to the In and Ag substitution, the electronic band structure was unfolded to primitive cell by using the VASPKIT code[12].

Lorenz number calculations: An estimation of L can be made using a single parabolic band (SPB) model with acoustic phonon scattering, resulting in a L with a deviation of less than 10% as compared with a more rigorous single non-parabolic band and multiple bands model calculation. Since the L was used to estimate the lattice thermal conductivity through the Wiedemann-Franz relation, thus, L would not change the total thermal conductivity and final ZT. The Lorenz number is given by the formula:

$$L = \left(\frac{k_B}{e}\right)^2 \left(\frac{(r+7/2)F_{r+5/2}(\eta)}{(r+3/2)F_{r+1/2}(\eta)} - \left[\frac{(r+5/2)F_{r+5/2}(\eta)}{(r+3/2)F_{r+1/2}(\eta)}\right]^2\right) \backslash *$$

MERGEFORMAT (15)

where k_B is the Boltzmann constant, e is the electric charge, r is the scattering rate, and η refers to the reduced Fermi energy.

Table S1. Densities of $(SnSe)_{1-x}(AgInSe_2)_x$ (x = 0, 0.01, 0.015, 0.02, and 0.025) and $(Sn_{1-y}Ge_ySe)_{0.985}(AgInSe_2)_{0.015}$ (y = 0.005, 0.0075, 0.01, and 0.0125) samples.

Compositions	Measured densities ρ (g cm^{-3})
x = 0	5.70
x = 0.01	5.72
x = 0.015	5.70
x = 0.02	5.71
x = 0.025	5.70
y = 0.005	5.73
y = 0.0075	5.70
y = 0.01	5.71
y = 0.0125	5.71
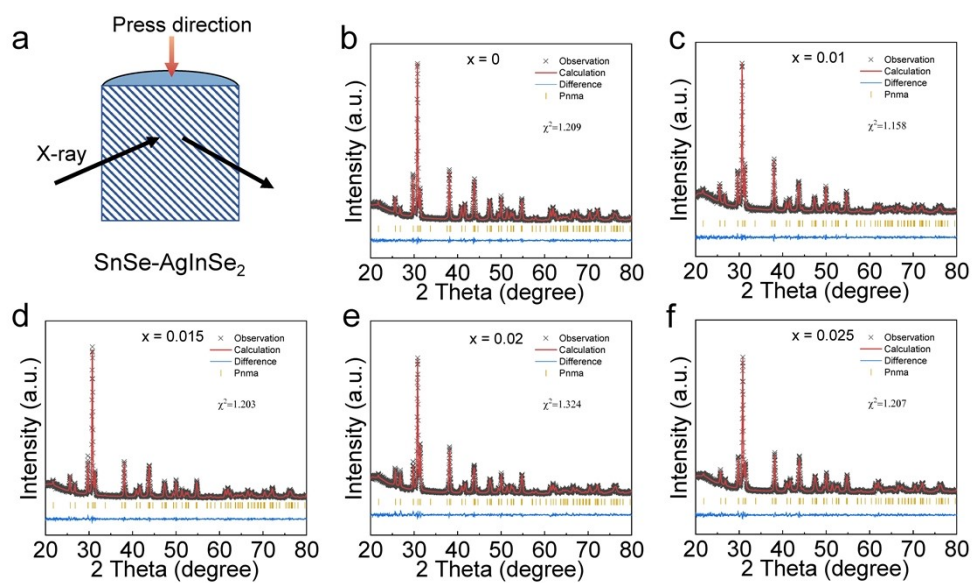
Figure S1. (a) PXRD measurement direction schematic; (b) Room-temperature PXRD patterns and Rietveld refinements for $(SnSe)_{1-x}(AgInSe_2)_x$ (x = 0, 0.01, 0.015, 0.02, and 0.025).
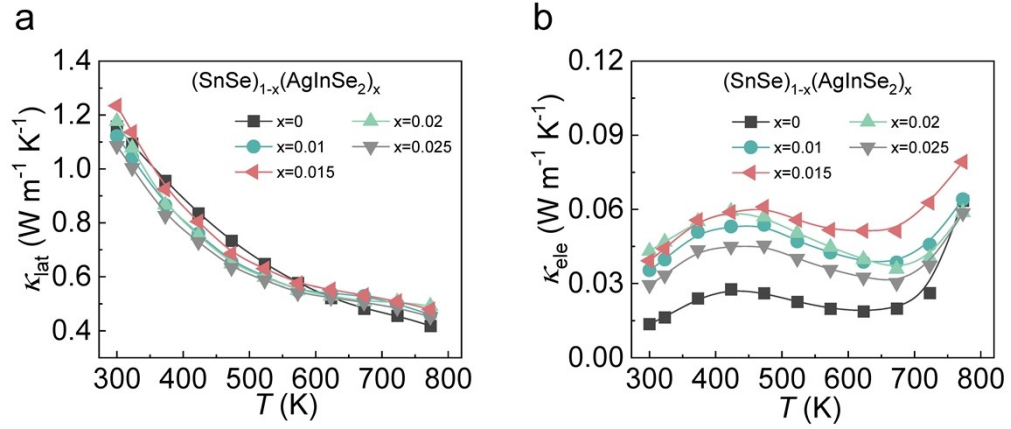
Figure S2. Thermal transport properties of SnSe-AgInSe$_2$ samples with rising temperature (a) Lattice thermal conductivities; (b) Electronic thermal conductivities.
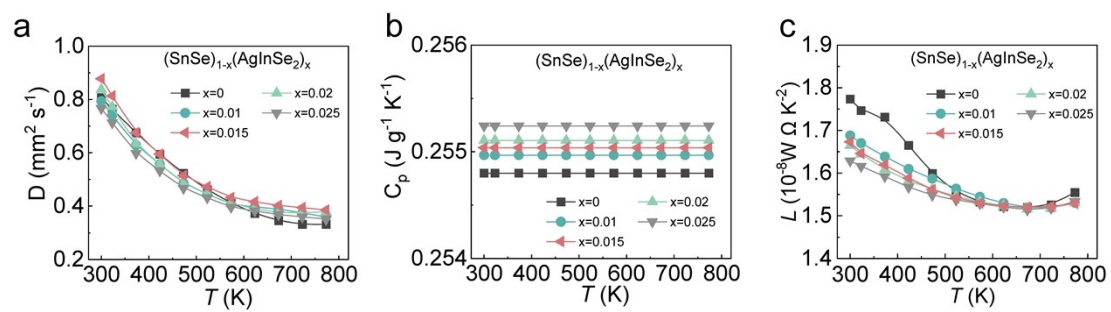
Figure S3. Thermal transport properties of SnSe-AgInSe$_2$ samples with rising temperature (a) Thermal diffusion coefficient; (b) Specific heat; (c) Lorenz number.
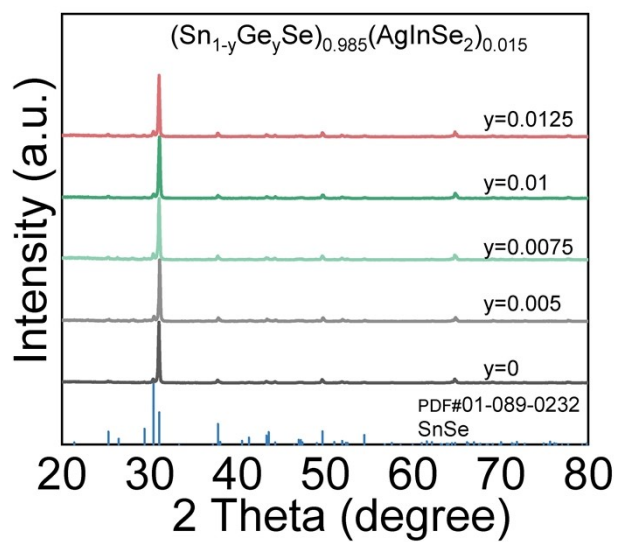
Figure S4. PXRD patterns of $(Sn_{1-y}Ge_ySe)_{0.985}(AgInSe_2)_{0.015}$ (y = 0, 0.005, 0.0075, 0.01, and 0.0125).

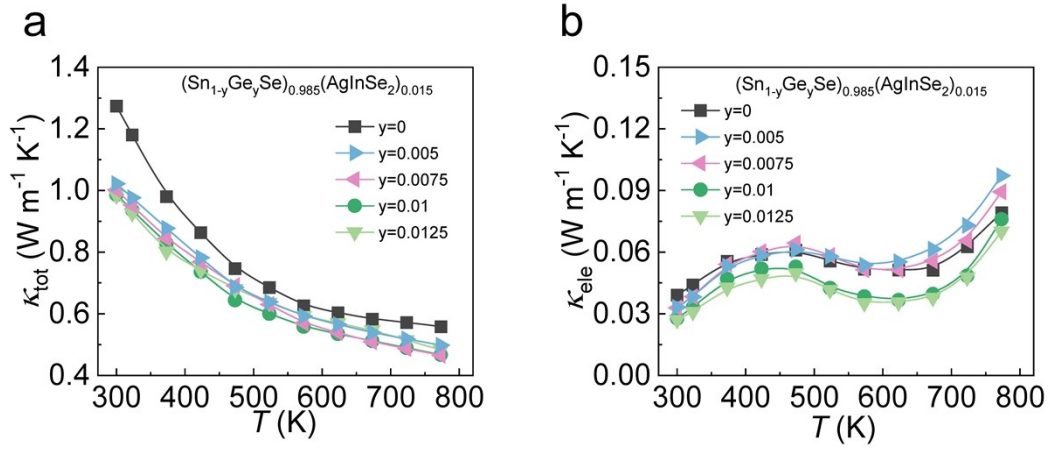**Figure S5**. Thermal transport properties of $(Sn_{1-y}Ge_ySe)_{0.985}(AgInSe_2)_{0.015}$ samples with rising temperature (a) Total thermal conductivities; (b) Electronic thermal conductivities.
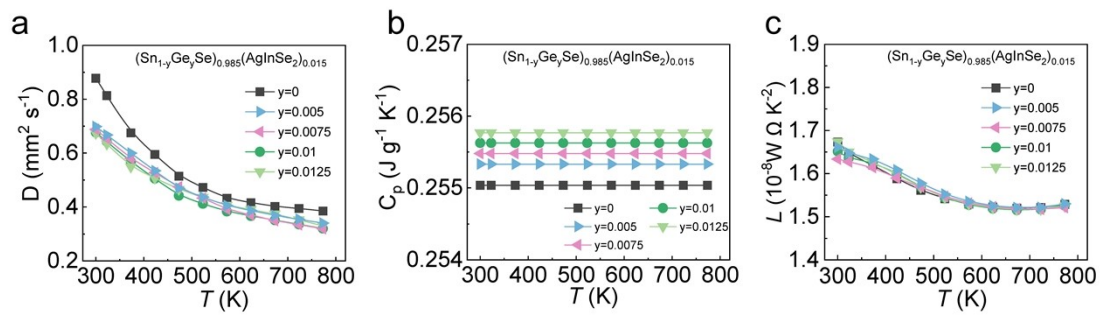
Figure S6. Thermal transport properties of $(Sn_{1-y}Ge_ySe)_{0.985}(AgInSe_2)_{0.015}$ samples with rising temperature (a) Thermal diffusion coefficient; (b) Specific heat; (c) Lorenz number.

Reference

1. J. Callaway, *Phys. Rev.*, 1959, **113**, 1046-1051.

2. J. Callaway, and H.C. von Baeyer, *Phys. Rev.*, 1960, **120**, 1149-1154.

3. K. Kurosaki, A. Kosuga, H. Muta, M. Uno, and S. Yamanaka, *Appl. Phys. Lett.*, 2005, **87**, 061919.

4. C.L. Wan, W. Pan, Q. Xu, Y.X. Qin, J.D. Wang, Z.X. Qu, and M.H. Fang, *Phys. Rev. B*, 2006, **74**, 144109.

5. Y.-L. Pei, J. He, J.-F. Li, F. Li, Q. Liu, W. Pan, C. Barreteau, D. Berardan, N. Dragoe, and L.-D. Zhao, *Npg Asia Mater*, 2013, **5**, e47.

6. Y. Xiao, W. Li, C. Chang, Y. Chen, L. Huang, J. He, and L.-D. Zhao, *J. Alloys Compd.*, 2017, **724**, 208-221.

7. C. Wan, Z. Qu, Y. He, D. Luan, and W. Pan, *Phys. Rev. Lett.*, 2008, **101**, 085901.

8. G.J. Tan, F.Y. Shi, H. Sun, L.-D. Zhao, C. Uher, V.P. Dravid, and M.G. Kanatzidis, *J. Mater. Chem. A*, 2014, **2**, 20849-20854.

9. P.E. Blochl, *Phys. Rev. B*, 1994, **50**, 17953-17979.

10. J.P. Perdew, A. Ruzsinszky, G.I. Csonka, O.A. Vydrov, G.E. Scuseria, L.A. Constantin, X. Zhou, and K. Burke, *Phys. Rev. Lett.*, 2008, **100**, 136406.

11. Z. Wu, and R.E. Cohen, *Phys. Rev. B*, 2006, **73**, 235116

12. V. Wang., N. Xu., J.-C. Liu., G. Tang, and W.-T. Geng., *Comput. Phys. Commun.*, 2021, **267**, 108033.